HHS Public Access

Author manuscript

ACS Appl Bio Mater. Author manuscript; available in PMC 2024 January 13.

Published in final edited form as:

ACS Appl Bio Mater. 2023 August 21; 6(8): 3257–3265. doi:10.1021/acsabm.3c00354.

Carbon Coated Iron–Cobalt Nanoparticles for Magnetic Particle Imaging

Raj Kumar[#],
Department of Pharmaceutical Sciences, School of Pharmacy, The University of Texas El Paso, El Paso, Texas 79902, United States; Department of Biomedical Engineering, The University of Texas El Paso, El Paso, Texas 79968, United States

Md Nurul Huda[#],
Department of Pharmaceutical Sciences, School of Pharmacy, The University of Texas El Paso, El Paso, Texas 79902, United States;

Ahsan Habib,
Department of Chemistry and Biochemistry, College of Sciences, The University of Texas El Paso, El Paso, Texas 79968, United States

Md Nafiujjaman,
Department of Biomedical Engineering, Institute for Quantitative Health Science and Engineering, Michigan State University, East Lansing, Michigan 48824, United States

Hyun-Joo Woo,
Department of Biomedical Engineering, Institute for Quantitative Health Science and Engineering, Michigan State University, East Lansing, Michigan 48824, United States

Taeho Kim,
Department of Biomedical Engineering, Institute for Quantitative Health Science and Engineering, Michigan State University, East Lansing, Michigan 48824, United States

Md Nurunnabi
Department of Pharmaceutical Sciences, School of Pharmacy, The University of Texas El Paso, El Paso, Texas 79902, United States; Department of Biomedical Engineering and Border Biomedical Research Center, The University of Texas El Paso, El Paso, Texas 79968, United States

Abstract

Corresponding Author: **Md Nurunnabi** – Department of Pharmaceutical Sciences, School of Pharmacy, The University of Texas El Paso, El Paso, Texas 79902, United States; Department of Biomedical Engineering and Border Biomedical Research Center, The University of Texas El Paso, El Paso, Texas 79968, United States; Phone: 915-747-8335; mnurunnabi@utep.edu.

[#]Author Contributions

R.K. and M.N.H. contributed equally to this paper. R.K.: Investigation, Methodology, Writing-Original draft preparation; M.N.H.: Conceptualization, Investigation, Methodology, Writing-Original draft preparation; A.H.: Investigation, Reviewing; M.N.: Investigation, Methodology, Reviewing; T.K.: Investigation, Supervision, Reviewing and Editing; M.N.: Conceptualization, Investigation, Supervision, Reviewing and Editing.

Complete contact information is available at:
https://pubs.acs.org/10.1021/acsabm.3c00354

The authors declare no competing financial interest.

Magnetic particle imaging (MPI) is an emerging imaging modality that provides direct and quantitative mapping of iron oxide tracers. To achieve high sensitivity and good spatial resolution images, a magnetic nanoparticle with a higher contrast intensity needs to be developed. Currently, a majority of MPIs being developed for potential clinical application are composed of iron oxide nanoparticles with a spherical shape. In this project, we intend to report development of high-performance carbon (C) coated iron–cobalt (FeCo) nanoparticles (FeCo/C) and investigate their feasibility as a MPI agent. We have synthesized FeCo/C through a facile and simple method at mild temperature that is safe, easy, and up-scalable. We studied the structural and functional relationships and biocompatibility of this MPI agent in vitro. However, to enhance the aqueous solubility and biocompatibility, the surface of FeCo/C was modified with polyethylene glycol (PEG). We found that variation in the ratio of Fe and Co plays a vital role in their physical properties and functionality. In vitro imaging confirms that the Fe_3Co_1/C nanoparticle has highly competitive MPI intensity compared to VivoTrax, a commercially available MPI agent. Confocal laser scanning microscopy imaging with Rhodamine B labeled FeCo/C displays cellular internalization by the A375 cancer cells. The in vitro toxicity analysis concludes that there is no significant toxicity of FeCo/C nanoparticles. Therefore, the newly developed MPI agent holds strong promise for biomedical imaging and could be further validated in vivo in small animals.

Graphical Abstract

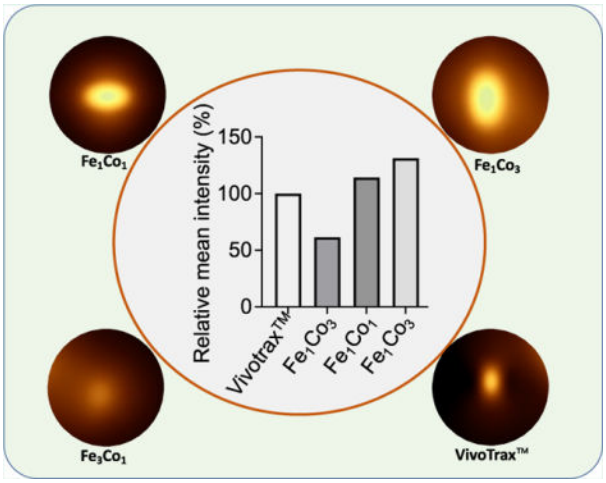

Keywords

MPI; metal nanoparticles; bioimaging; magnetic nanoparticles; iron–cobalt nanoparticles

INTRODUCTION

Biomedical imaging plays a vital role in the clinic to diagnose the diseases condition, pathology, and even therapeutic progress.[1] The medical imaging technologies such as X-ray,[2] PET (Positron emission tomography),[3] CT (computerized tomography)[4] scan, and magnetic resonance imaging (MRI)[5] visualizes lesion, blood flow, discriminating diseased tissues from normal tissues in the human body.[6] The diagnosis by medical imaging technologies offers to detect the stage of diseases and timely monitor the progress of

treatment.[7] Among the medical imaging technologies, MRI shows the most reliable and deep tissue imaging feasibility but crucially depends on magnetic field homogeneity.[8] MRI images also suffer highly from a lack of contrast between signal-to-noise.

Recently, MPI (magnetic particle imaging), a novel and new medical imaging technology has been developed and emerged with higher feasibility and effectivity than MRI.[9–1112] What's particularly fascinating about MPI imaging is its capability and quality does not rely on magnetic field homogeneity, and MPI can still produce accurate and high-quality images. MPI is a promising in vivo imaging technology that exploits the nonlinear magnetic response of superparamagnetic nanoparticles. MPI directly measures the magnetization of magnetic particle tracers,[9,1312] and is sensitive and fast with spatial and temporal resolutions. Theoretically, MPI technology produces quantitative information with an acquisition time less than 0.1 s and spatial resolution below 1 mm.[14] It provides high quality and real-time imaging. Since tissue and organ components are diamagnetic, they appear transparent in MPI measurement. This results in the elimination of background signal and hence producing images with exceptional positive contrast.[15] Moreover, MPI scans are conducted at low frequency magnetic fields, which leads to zero attenuation, implying this imaging method of quantitative at any depth.[16]

The major challenge for the clinical translation of MPI has been the development of sustainable and biocompatible magnetic nanoparticles. This is because the magnetic response to an external field depends on the properties of the magnetic nanoparticles and the surrounding solvent. Magnetic nanoparticles properties such as core size, size distribution, phase and crystallinity decide the external magnetic response.[13] However, the nanoparticles of iron or metal are unstable and get oxidized in the presence of air or water.[9] Optimized magnetic nanoparticles generate MPI maps with a high signal intensity and resolution. However, their clinical use is limited due to lack of widely available technology and tools on top of concerns related to biosafety.[10] To develop a new type of MPI agent that can overcome the existing concerns, we have synthesized an iron–cobalt (FeCo) nanoparticle with various ratios such as 1:3, 1:1, and 3:1, and the respective nanoparticles are denoted as Fe_1Co_3/C, Fe_1Co_1/C, and Fe_3Co_1/C. We have synthesized the iron–cobalt derivatives from tissue paper, iron nitrate, and cobalt nitrate with high heat. Finally, the nanoparticle was coated with carbon via carbonization with higher heat in the furnace.

The major limitations of using metal nanoparticles in biomedical applications, including MPI, are their poor solubility in aqueous solutions and their susceptibility to oxidation in the presence of air. Polymeric coating techniques play a vital role in improving the hydrophilicity of nanoparticles and protecting them from oxidation. Interestingly, chemical stability increases when two metal interacted with each other.[17] Further, to increase stability and dispersibility of the nanoparticles, the surface of the FeCo/C nanoparticles was modified with PEG. For confocal imaging, we further conjugated with Rhodamine B (RhB), which is represented as FeCo/C@PEG/RhB nanoparticles.[13] In addition, we conduct a comprehensive and systematic evaluation of the morphological, structural, and functional properties of the magnetic nanoparticles. In vitro cytotoxicity tests were conducted using skin cancer cell lines A375. The magnetic nanoparticle internalization and accumulation in the cell cytoplasm were observed in confocal imaging. What is even more intriguing is that

MPI imaging of FeCo/C nanoparticles showed 135% higher intensity than commercially available MPI agent VivoTrax. This highlights the potential of FeCo/C nanoparticles as highly efficient contrast agents for MPI imaging.

MATERIALS AND METHODS

Materials.

Polyethylene glycol (PEG 1000) was purchased from Spectrum RX (New Brunswick, NJ), Rhodamine B (RhB) 1-ethyl-3-(3-dimethylaminopropyl)-1-carbodiimide hydrochloride (EDC.HCl, abbreviated as EDC), dichloromethane (DCM), *N*-hydroxy succinimide (NHS), and iron nitrate ($Fe(NO_3)_3$. $6H_2O$), and cobalt nitrate ($Co(NO_3)_2$. $6H_2O$), Hoechst, propidium iodide, and PKH67 cell staining dye were purchased from Sigma-Aldrich (St. Luis, MO). MTT assay kit, Dulbecco's Modified Eagle Medium, fetal bovine serum, and penicillin–streptomycin solution were purchased from Thermo Fisher (Waltham, MA). All the reagents were used as received. The source of Deionized (DI) water is Millipore Milli-Q Reference Ultrapure Water Purification System. Tissue paper was purchased from a local store.

Synthesis of the Electrocatalysts.

Initially, 1.5 g of each metal salt was dissolved in 10 mL of DI (deionized water) water in a 100 mL beaker. Subsequently, 3 g of tissue paper (in the form of tiny pieces) was placed into the metal salt solution, and the mixture was sonicated so that the Fe^{3+} and Co^{2+} ions were adsorbed on the tissue paper, followed by heating the mixture at 100 °C to remove all the water molecules. Afterward, the mixture was carbonized at 800 °C for 4 h in a tube furnace, and the heating rate was set to 5 °C min^{-1}.[18] The black product of bimetallic nanoparticles was collected and named Fe_1Co_1/C. Two other bimetallic electrocatalysts were also prepared, namely, Fe_3Co_1/C and Fe_1Co_3/C, concerning the (w/w) % of the iron and cobalt salts that were used during the synthesis process.

Characterization FeCo/C Nanoparticles.

The as-synthesized FeCo/C nanoparticles were first characterized using the X-ray diffraction (XRD) technique with a Cu Kα radiation source in 2θ = 20–80° at a scan rate of 5° min^{-1} (Model: Bruker D8 advanced diffractometer). Transmission electron microscopy (TEM) analysis was carried out on a Hitachi H-7650 microscope to further inspect the morphology of the nanoparticles.

PEGylation of the FeCo/C Nanoparticles.

We have prepared three different iron–cobalt compounds such as Fe_1Co_3/C, Fe_1Co_1/C, and Fe_3Co_1/C. Further, to make it more biocompatible, the FeCo/C nanoparticles were coated with PEG according to the method reported elsewhere.[19,20] In brief, the PEG solution was prepared by dissolving them into DI water (5%). In a separate beaker, the FeCo/C nanoparticles were added to water and stirred for 15 min to facilitate their dispersion, followed by a 15 min sonication in the water bath. Then an aqueous solution of PEG was added to the dispersed FeCo/C nanoparticles with slow agitation. The mixture of iron–cobalt and PEG was centrifuged for 10 min after 1 h of stirring at room temperature. Further, the

unconjugated excess of PEG was removed by filtration with standard Whatman filter paper. The resulting PEG coated iron–cobalt nanoparticles (Fe_1Co_3/C@PEG, Fe_1Co_1/C@PEG, and Fe_3Co_1/C@ PEG), were dried by lyophilizing using a freeze-dryer. The next day, PEGylated FeCo/C were collected in a separate vial.

Next, 5 mg of FeCo/C@PEG was measured and redispersed in DI water. We measured FeCo/C@PEG: RhB: EDC: NHS at a molar ratio of 1:1:1:1. After the overnight reaction, the samples were collected and centrifuged at 3000 rpm for 10 min to spin down the FeCo/C@PEG/RhB nanoparticle and to remove the unconjugated RhB, EDC, and NHS. Then the precipitated nanoparticles were collected by discarding the supernatant. After that, the precipitants were dried using a freeze-dryer for 24 h.

Characterization of the PEGylated FeCo/C Nanoparticles.

For characterization, the nanoparticles with and without a PEG coating were dissolved and diluted with DI water at 1 mg/mL concentration. Particle size (diameter in nm), zeta potentials (mV), and polydispersity index (PDI) were measured using dynamic light scattering (DLS).[21–23] Again, all six nanoparticles were dissolved in DI water and prepared at a concentration of 0.1 mg/mL for zeta potential measurement.[24,25] Both DLS and the zeta potential were measured separately and triplicated for each sample for statistical significance. Further, colloidal stability of the PEGylated nanoparticle was investigated upon dispersion in PBS and incubation for 5 h at room temperature. Particle size dispersion and surface zeta potential were measured at each hour to monitor agreegation.

MPI Spectroscopy of FeCo/C@PEG Nanoparticles.

MPI agents sensitivity of FeCo/C nanoparticles and VivoTrax (Purchased from Magnetic Insight Inc., CA, USA) were analyzed by Momentum MPI scanner (Magnetic Insight Inc., CA, USA).[14,26] 30 μL of both nanoparticles were dissolved in an aqueous solution and were transferred to 600 microtubes for measurement by MPS. 2D projection scans were performed, beginning with the default setting (5.7 T/m gradient).[27] Mean sensitivity was analyzed by using ImageJ.

Live–Dead Assay.

To evaluate the cellular toxicity of FeCo/C, a live–dead assay was conducted upon 24 h of incubation with four different concentrations of the nanoparticles.[28,29] A375 cells were added in each well of 12 wells plate and seeded for 36 h to let the cells attach on the surface. Cells were cultured with DMEM with 10% FBS and 1% penicillium-streptomycin in 5% CO_2 and 95% air at 37 °C. FeCo/C nanoparticles were added at a concentration of 0.1 mg/mL, 0.05 mg/mL, 0.025 mg/mL, and 0.0125 mg/mL concentration and incubated for 24 h. After conincubation, the cell was gently washed three times with 1× PBS and stained the cells with Hoechst (1:500) and propodeum iodide (1:500) for 20 min. After staining the live and dead cells, we rewashed them three times with 1× PBS. Finally, the cells were fixed with 4% paraformaldehyde for 15 min. After fixation, the plates were scanned using a fluorescent microscope EVOS 5000 imaging system to take images in bright, violet, and red laser fields. Hoechst and propodium iodide were used to stain both live-cell nuclei and dead cell's double-stranded DNA, respectively.[30,31] Images were collected at 20× magnification

and exposure, gaining similar settings. All images were analyzed using ImageJ software by NIH.

Cellular Toxicity Assay.

The MTT cell viability assay was conducted to evaluate cytoxicity of FeCo/C before and after PEG coating.[32] Two 96-well plates with 3000 cells per well of A375 cells were prepared for the MTT assay. Cells were maintained with DMEM with 10% FBS and 1% penicillium–streptomycin as the cell culture medium. The nanoparticles were added 36 h after seeding the cell on the well. This experiment was designed to observe cell cytotoxicity based on concentration and duration of incubation. In brief, after seeding, the cells were treated at 100, 50, 25, 12.5, and 6.25 μg/mL for 6 h. After cotreatment, the medium was replaced with a fresh 100 μL in each well. Then 10 μL of MTT solution (3-(4,5-dimethylthiazol-2-yl)-2,5-diphenyltetrazolium bromide, 12 mM) was added with each well and mixed with a pipet up and down. We also included a negative control by adding 10 μL of the MTT stock solution to 100 μL of the medium alone. Then each plate was incubated for 4 h. After 4 h of incubation, 25 μL of the medium was removed from each well, followed by addition of 50 μL of DMSO to each well.

Then the plate was incubated for 10 min in incubator. After 10 min of incubation, we pipet up and down to remix each sample, and then absorbance was recorded at 540 nm using a 96-plate reader. Cell viability was calculated based on absorbance value according to the formula below. All data are tabulated and statistically analyzed by using the Prism Graph Pad software.

$$\text{cell viability}\,(\%) = \left[\frac{\overline{A_{\text{sample}}} - \overline{A_{\text{blank}}}}{\overline{A_{\text{control}}} - \overline{A_{\text{blank}}}}\right] \times 100\%$$

Cell Internalization Assay of FeCo/C@PEG.

To examine cell internalizations profile of PEGylated FeCo/C, each nanoparticle was labeled with fluorescent dye Rhodamine B.[33] Human skin melanoma cell A375 were seeded in each well of a Nunc lab-tech II chambered glass cover system and allowed to sediment for 36 h. After that, RdB labeled FeCo/C nanoparticles were added at a concentration of 1 mg/mL and coincubated for 6 h. After coincubation, the cells were washed three times with 1× DPBS to remove nanoparticles that were not taken up by the cells. Subsequently, the cells were stained with Hoechst (1:500) and PKH67 (1:500) for 20 min each in 1× DPBS dilution to stain the nucleus and membrane. After the staining process, the cells were fixed with 4% paraformaldehyde for 15 min. Then we replaced the wells with fresh 1× PBS and took the image in a fluorescent imaging microscope using the EVOS 5000 imaging system. Finally, the images were processed by using ImageJ software for quantitative analysis.

RESULTS AND DISCUSSION

Structural Characterization of FeCo/C.

Figure 1A shows the synthesis method of the FeCo/C derivatives. As seen, the synthesis of FeCo/C nanoparticles was accomplished via a two-step strategy that includes the adsorption of the Co^{2+}/Fe^{3+} ions into tissue paper, followed by pyrolysis. During the pyrolysis step, the tissue paper serves as a carbon source, while the metal salts act as a metal source to form the final carbon encapsulated FeCo structure. The crystalline structure of the bimetallic nanoparticles was first investigated using XRD, as seen in Figure 1B. The XRD pattern showed three characteristic diffraction peaks in all cases at ~30.89°, 36.45°, and 45.92°, and these peaks correspond to the 110, 200, and 211 crystal planes of the body entered cubic FeCo nanoparticles, confirming the successful formation of the FeCo/C nanoparticles. However, the diffraction pattern did not show any additional peaks, suggesting the high purity of the as-prepared nanoparticles. We have also confirmed that the crystal planes of each nanoparticle after PEGylation. The results represented in Figure 1B shows that the crystal property of the nanoparticle remained the same even after PEGylation as depicted by the XRD spectrum.

PEGylation of FeCo/C and Characterization.

FeCo/C nanoparticles are, in general, smaller in diameter and hydrophobic. To improve the aqueous solubility and biocompatibility by reducing the toxicity of FeCo/C nanoparticles, the individual nanoparticles were modified with PEG. Figure 2A shows the PEGylation method. Physical mixing in association with bath sonication was used to facilitate the PEGylation of the FeCo/C nanoparticles. The unconjugated and free PEG were removed using centrifugation and filtration. Finally, lyophilization using a freeze-dryer was used to obtain the dried PEGylated FeCo/C nanoparticles. Upon coating with PEG, the hydrodynamic size of the FeCo/C nanoparticles was increased 50% in diameter as measured by DLS (Figure 2B). The sizes of the PEGylated nanoparticles were observed as larger in diameter compared to naked nanoparticles, which is a clear indication of successful surface modification. Next, we compare surface zeta potentials between uncoated and coated FeCo/C compounds. Surface zeta potentials determine how FeCo/C nanoparticles will interact with the cell membrane. Zeta potential value of Fe_1Co_3/C nanoparticle also confirmed presence of PEG on the surface as values changed from +6 mV to −3 mV. Along the same line, zeta potential values for Fe_1Co_1/C and Fe_3Co_1/C nanoparticles changes from −2 mV to −6 mV, and from −4 mv to −1.5 mV after PEGylation, respectively (Figure 2C). The polydispersity index (PDI), which determines how uniform the particles are, shows a PDI value range from 0.6 to 0.9 (Figure 2D).

Then the morphology of the nanoparticles was inspected using TEM. As seen in Figure 3, the FeCo/C nanoparticles are within 100 nm in diameter in range but not uniformly distributed and distributed in aqueous solution (PBS). However, after PEG coating the FeCo particles have been seen to increase their size but improve dispersibility significantly. The gray area on the outer surface of the particle also confirms successful coating of the nanoparticle with PEG (Figure 3).

Colloidal stability of the nanoparticles is very critical to predict their aggregation and dispersibility behavior upon dissolution in solution. In this work, we dissolved the PEGylated FeCo/C nanoparticles in PBS and incubated them at room temperature for a certain duration. We have observed that the size distribution of the nanoparticle tends to increase as the duration of incubation increased, which is a clear indication of aggregation. However, the size increment was observed by only 40% upon 5 h of incubation, which does not indicate any significant changes (Figure 4). Zeta potential value indicates the surface zeta potential of the nanoparticles. The data presented in Figure 4 does not show any significant changes in zeta potential, indicating that the nanoparticles are very stable for at least 5 h upon incubation in PBS at room temperature.

MPI Agents Sensitivity of FeCo/C.

In MPI, the inexpensive compound with better magnetic signaling and high spatial resolution is better accepted in imaging applications.[17] FeCo nanoparticles are known to show high magnetic saturation compared to iron oxide (Fe_3O_4), which leads to a high intensity of the MPI signal. We envision that the FeCo/C nanoparticle will facilitate MPI, and higher iron content will provide higher contrast intensity. With this, we have conducted in vitro MPI and compared the results with the FDA-approved commercially available MPI agent VivoTrax. The in vitro phantom imaging study shows that Fe_1Co_3/C, Fe_1Co_1/C, and Fe_3Co_1/C are 60, 120, and 135% more efficacious, respectively, compared to VivoTrax. To demonstrate MPI sensitivity of the newly prepared Fe_3Co_1/C nanoparticles, we analyzed MPI sensitivity by a Momentum MPI scanner where commercial VivoTrax was used as control (Figure 5). Based on the images and analyzed data, Fe_3Co_1/C with a higher amount of iron results in higher sensitivity, thereby giving brighter and better magnetic images.

Cell Toxicity Assay of FeCo/C (Live & Dead Assay).

Bioaccumulation, bioavailability, and bioabsorption are critical parameters that help to assess the biosafety of the nanoparticles prior to considering for biomedical applications. Therefore, to assess the cytocompatibility of the FeCo/C nanoparticles, we have coincubated the PEGylated FeCo/C nanoparticles with skin cancer cell A375. Iron compounds are directly toxic to targeted organs and can cause direct caustic injuries like vomiting, abdominal pain, and gastrointestinal mucosa.[34] Also, free iron can enter the cell and accumulate within mitochondria. This can disrupt catalyzed lipid peroxidation, oxidative phosphorylation, and form free radicals, and thereby leading to cell death.[35] This assay evaluates if the FeCo/C nanoparticles are cytotoxic and compares the cytotoxicity among the derivatives of FeCo/C nanoparticles. Each nanoparticle was seeded at a concentration of 100, 50, 25, and 12.5 μg/mL and coincubated for 24 h. For Fe_1Co_3/C nanoparticles, we observed higher cell death as quantified by propidium iodide for 100, 50, and 25 μg/mL concentrations. However, we have observed 99% cell viability at a 12.5 μg/mL concentration. We conclude that the optimal concentration of Fe_1Co_3/C will be around 12.5 μg/mL to avoid cytotoxicity (Figures 6 and 7). In Figure 6, we have observed Fe_1Co_1/C shows lower toxicity at concentrations of 50, 25, and 12.5 μg/mL. Finally, for the Fe_3Co_1/C nanoparticle, cell viability was around 90% and 95% for the concentration of 25 and 12.5 μg/mL. The toxicity and dose evaluation study observed with the Fe_1Co_1/C compound shows lower toxicity at 50, 25, and 12.5 μg/mL concentration compared to the other two

derivatives. Moreover, Fe_1Co_3/C and Fe_3Co_1/C nanoparticles can also be applied at doses lower than 25 μg/mL concentration to avoid any toxicity issues during imaging application (Figure 8).

Cell-Viability Assay of PEGylated FeCo/C Nanoparticles.

Biomedical application of newly developed nanomaterials is required through studies to investigate their biocompatibility, cytotoxicity, and biodegradability. Though, PEG is an FDA-approved biopolymer for drug delivery and biomedical applications, we sought to investigate in vitro cytotoxicity of the PEGylated FeCo/C nanoparticles. A 3-(4,5-dimethylthiazol-2-yl)-2,5-diphenyltetrazolium bromide (MTT) assay was conducted to evaluate cytotoxicity with various concentrations of the nanoparticles.[36] PEGylated FeCo/C nanoparticles (Fe_1Co_3/C, Fe_1Co_1/C, and Fe_3Co_1/C) were incubated with A375 cells for 6 h with concentrations of 100, 50, 25, 12.5, and 6.25 μg/mL. The Fe_1Co_1/C and Fe_3Co_1/C nanoparticles are comparatively less cytotoxic to A375 cells than Fe_1Co_3/C. Cell viability for Fe_1Co_3/C shows that the viability went down to 80% at a concentration of 100 μg/mL but went up to 95% at a concentration of 6.25 μg/mL (Figure 9). FeCo/C nanoparticles are generally coated to reduce toxicity and aggregations, and we have observed the expected results in this case.[37] PEG is a stable, biocompatible hydrophilic compound that has been used for drug and gene delivery for various disease models.[38] PEG accumulation can also reduce phagocytic capture of FeCo/C nanoparticles and increase systemic circulation, enabling FeCo/C nanoparticles to accumulate a targeted tissue of interest.[39] Figure 5 shows that due to PEG coating, cell viability values were increased from 85 to 95% to 90–99% for concentrations of 25, 12.5, and 6.25 μg/mL. Our investigation validates that with PEG coating, FeCo/C nanoparticles can decrease their toxicity.

Fluorescent Imaging of RhB Coated Iron–Cobalt Compound Intake in Healthy and Cancer Cells.

We envision that a PEG coating will enhance aqueous solubility of FeCo/C nanoparticles as well as enhance cellular uptake via the RES system. For cellular internalization study and to visualize the uptaken nanoparticle, we have coincubated A375 cells with RhD labeled FeCo/C@PEG nanoparticles and investigated them under a fluorescent microscope (Figure 10). We have observed that regardless of the core composition of the particles, cellular uptake and internalization were very much identical. The cells were stained with Hoechst (live nucleus) to specifically indicate subcellular localization of the FeCo/C nanoparticles. Figure 10 shows that FeCo/C nanoparticles were successfully internalized by the A375 cell, and in some cases, the nanoparticles were even found within the nucleus, which is an indication of the particle's ability to be internalized by the cell.

CONCLUSIONS

In summary, we have synthesized, characterized, and observed the feasibility of FeCo/C as a potential MPI agent. The FeCo/C nanoparticles synthesized with pyrolysis were found to be uniformly dispensed. The average particle size of the nanoparticles was observed to be ~15–20 nm in diameter. The results demonstrated that the ratio of Fe and Co plays a critical role in the physicochemical properties of FeCo/C. Further, the PEG-coating provided great

chemical stability and dispersibility of FeCo/C in aqueous solution. First, the surface coating restricts FeCo/C nanoparticles from aggregating in the physiological system. Second, the coating prevents the immunogenic reaction of FeCo/C nanoparticles inside the physiological system. Third, the surface coating further acts as an anchoring point that facilitate the attachment of functional groups or fluorescent agents.[17] For in vivo applications, PEG coating is a proven strategy that increases systemic circulation of FeCo/C nanoparticles in the blood.[40] Upon injection of FeCo/C nanoparticles, FeCo/C nanoparticles are opsonized, and subsequent uptake occurs by the reticuloendothelial system (RES). Cell studies demonstrate that PEG-coated FeCo/C maintains excellent biocompatibility and a good cellular uptake profile. Confocal imaging confirmed that FeCo/C nanoparticles penetrate the cell membrane and accumulate within A375 skin cancer cells. More importantly, Fe_3Co_1/C exhibited 135% stronger MPI signals than commercially available MPI agent VivoTrax.

ACKNOWLEDGMENTS

We acknowledge funding by the Cancer Prevention Research Institute of Texas (CPRIT) through the Texas Regional Excellence in Cancer Award (TREC) under Award No. RP210153, and National Institutes of Health (NIH) under Award No R03OD032624. The contents of this paper are solely the authors' responsibility and do not necessarily represent the official views of NIH.

REFERENCES

(1). Goel S; Chen F; Cai W Synthesis and Biomedical Applications of Copper Sulfide Nanoparticles: From Sensors to Theranostics. Small 2014, 10 (4), 631–645. [PubMed: 24106015]

(2). Oh MH; Lee N; Kim H; Park SP; Piao Y; Lee J; Jun SW; Moon WK; Choi SH; Hyeon T Large-Scale Synthesis of Bioinert Tantalum Oxide Nanoparticles for X-Ray Computed Tomography Imaging and Bimodal Image-Guided Sentinel Lymph Node Mapping. J. Am. Chem. Soc 2011, 133 (14), 5508–5515. [PubMed: 21428437]

(3). Duara R; Grady C; Haxby J; Sundaram M; Cutler NR; Heston L; Moore A; Schlageter N; Larson S; Rapoport SI Positron Emission Tomography in Alzheimer's Disease. Neurology 1986, 36 (7), 879–887. [PubMed: 3487046]

(4). Sonaje K; Chuang EY; Lin KJ; Yen TC; Su FY; Tseng MT; Sung HW Opening of Epithelial Tight Junctions and Enhancement of Paracellular Permeation by Chitosan: Microscopic, Ultrastructural, and Computed-Tomographic Observations. Mol. Pharmaceutics 2012, 9 (5), 1271–1279.

(5). Kaushik A; Rodriguez J; Rothen D; Bhardwaj V; Jayant RD; Pattany P; Fuentes B; Chand H; Kolishetti N; El-Hage N; Khalili K; Kenyon NS; Nair M MRI-Guided, Noninvasive Delivery of Magneto-Electric Drug Nanocarriers to the Brain in a Nonhuman Primate. ACS Appl. Bio Mater 2019, 2 (11), 4826–4836.

(6). Leff DR; Warren OJ; Enfield LC; Gibson A; Athanasiou T; Patten DK; Hebden J; Yang GZ; Darzi A Diffuse Optical Imaging of the Healthy and Diseased Breast: A Systematic Review. Breast Cancer Res. Treat 2008, 108 (1), 9–22. [PubMed: 17468951]

(7). Crosby D; Lyons N; Greenwood E; Harrison S; Hiom S; Moffat J; Quallo T; Samuel E; Walker I A Roadmap for the Early Detection and Diagnosis of Cancer. Lancet Oncol 2020, 21 (11), 1397–1399. [PubMed: 33031732]

(8). Na HB; Song IC; Hyeon T Inorganic Nanoparticles for MRI Contrast Agents. Adv. Mater 2009, 21 (21), 2133–2148.

(9). Song G; Kenney M; Chen YS; Zheng X; Deng Y; Chen Z; Wang SX; Gambhir SS; Dai H; Rao J Carbon-Coated FeCo Nanoparticles as Sensitive Magnetic-Particle-Imaging Tracers with Photothermal and Magnetothermal Properties. Nature Biomedical Engineering 2020 4:3 2020, 4 (3), 325–334.

(10). Billings C; Langley M; Warrington G; Mashali F; Johnson JA Magnetic Particle Imaging: Current and Future Applications, Magnetic Nanoparticle Synthesis Methods and Safety Measures. International Journal of Molecular Sciences 2021, Vol. 22, Page 7651 2021, 22 (14), 7651.

(11). Pablico-Lansigan MH; Situ SF; Samia ACS Magnetic Particle Imaging: Advancements and Perspectives for Real-Time in Vivo Monitoring and Image-Guided Therapy. Nanoscale 2013, 5 (10), 4040–4055. [PubMed: 23538400]

(12). Gleich B; Weizenecker J Tomographic Imaging Using the Nonlinear Response of Magnetic Particles. Nature 2005 435:7046 2005, 435 (7046), 1214–1217.

(13). Khandhar AP; Keselman P; Kemp SJ; Ferguson RM; Goodwill PW; Conolly SM; Krishnan KM Evaluation of PEG-Coated Iron Oxide Nanoparticles as Blood Pool Tracers for Preclinical Magnetic Particle Imaging. Nanoscale 2017, 9 (3), 1299–1306. [PubMed: 28059427]

(14). Ferguson RM; Khandhar AP; Kemp SJ; Arami H; Saritas EU; Croft LR; Konkle J; Goodwill PW; Halkola A; Rahmer J; Borgert J; Conolly SM; Krishnan KM Magnetic Particle Imaging with Tailored Iron Oxide Nanoparticle Tracers. IEEE Trans Med. Imaging 2015, 34 (5), 1077–1084. [PubMed: 25438306]

(15). Pablico-Lansigan MH; Situ SF; Samia ACS Magnetic Particle Imaging: Advancements and Perspectives for Real-Time in Vivo Monitoring and Image-Guided Therapy. Nanoscale 2013, 5 (10), 4040–4055. [PubMed: 23538400]

(16). Goodwill PW; Saritas EU; Croft LR; Kim TN; Krishnan KM; Schaffer DV; Conolly SM X-Space MPI: Magnetic Nanoparticles for Safe Medical Imaging. Adv. Mater 2012, 24 (28), 3870–3877. [PubMed: 22988557]

(17). Fang C; Zhang M Multifunctional Magnetic Nanoparticles for Medical Imaging Applications. J. Mater. Chem 2009, 19 (35), 6258–6266. [PubMed: 20593005]

(18). Tiwari A; Kumar R; Shefi O; Randhawa J Fluorescent Mantle Carbon Coated Core–Shell SPIONs for Neuroengineering Applications. ACS Appl. Bio Mater 2020, 3 (7), 4665–4673.

(19). Phadatare MR; Khot VM; Salunkhe AB; Thorat ND; Pawar SH Studies on Polyethylene Glycol Coating on NiFe2O4 Nanoparticles for Biomedical Applications. J. Magn Magn Mater 2012, 324 (5), 770–772.

(20). Yallapu MM; Foy SP; Jain TK; Labhasetwar V PEG-Functionalized Magnetic Nanoparticles for Drug Delivery and Magnetic Resonance Imaging Applications. Pharm. Res 2010, 27 (11), 2283–2295. [PubMed: 20845067]

(21). Li L; Nurunnabi M; Nafiujjaman M; Lee YK; Huh KM GSH-Mediated Photoactivity of Pheophorbide a-Conjugated Heparin/Gold Nanoparticle for Photodynamic Therapy. J. Controlled Release 2013, 171 (2), 241–250.

(22). Nurunnabi M; Khatun Z; Nafiujjaman M; Lee DG; Lee YK Surface Coating of Graphene Quantum Dots Using Mussel-Inspired Polydopamine for Biomedical Optical Imaging. ACS Appl. Mater. Interfaces 2013, 5 (16), 8246–8253. [PubMed: 23879568]

(23). Tanisaka H; Kizaka-Kondoh S; Makino A; Tanaka S; Hiraoka M; Kimura S Near-Infrared Fluorescent Labeled Peptosome for Application to Cancer Imaging. Bioconjug Chem. 2008, 19 (1), 109–117. [PubMed: 18163535]

(24). Nurunnabi M; Ibsen KN; Tanner EEL; Mitragotri S Oral Ionic Liquid for the Treatment of Diet-Induced Obesity. Proc. Natl. Acad. Sci. U. S. A 2019, 116 (50), 25042–25047. [PubMed: 31767747]

(25). Nurunnabi M; Cho KJ; Choi JS; Huh KM; Lee Y-k. Targeted Near-IR QDs-Loaded Micelles for Cancer Therapy and Imaging. Biomaterials 2010, 31 (20), 5436–5444. [PubMed: 20409581]

(26). Makela AV; Gaudet JM; Schott MA; Sehl OC; Contag CH; Foster PJ Magnetic Particle Imaging of Macrophages Associated with Cancer: Filling the Voids Left by Iron-Based Magnetic Resonance Imaging. Mol. Imaging Biol 2020, 22 (4), 958–968. [PubMed: 31933022]

(27). Makela AV; Gaudet JM; Schott MA; Sehl OC; Contag CH; Foster PJ Magnetic Particle Imaging of Macrophages Associated with Cancer: Filling the Voids Left by Iron-Based Magnetic Resonance Imaging. Mol. Imaging Biol 2020, 22 (4), 958–968. [PubMed: 31933022]

(28). Islam T; Huda MN; Ahsan MA; Afrin H; Salazar CJJ; Nurunnabi M Theoretical and Experimental Insights into the Possible Interfacial Interactions between β-Glucan and Fat

Molecules in Aqueous Media. J. Phys. Chem. B 2021, 125 (50), 13730–13743. [PubMed: 34902976]

(29). Huda MN; Deaguro IG; Borrego EA; Kumar R; Islam T; Afrin H; Varela-Ramirez A; Aguilera RJ; Tanner EEL; Nurunnabi M Ionic Liquid-Mediated Delivery of a BCL-2 Inhibitor for Topical Treatment of Skin Melanoma. J. Controlled Release 2022, 349, 783–795.

(30). Crowley LC; Marfell BJ; Waterhouse NJ Analyzing Cell Death by Nuclear Staining with Hoechst 33342. Cold Spring Harb Protoc 2016, 2016 (9), pdb.prot087205.

(31). Krishan A Rapid Flow Cytofluorometric Analysis of Mammalian Cell Cycle by Propidium Iodide Staining. J. Cell Biol 1975, 66 (1), 188–193. [PubMed: 49354]

(32). Afrin H; Huda MN; Islam T; Oropeza BP; Alvidrez E; Abir MI; Boland T; Turbay D; Nurunnabi M Detection of Anticancer Drug-Induced Cardiotoxicity Using VCAM1-Targeted Nanoprobes. ACS Appl. Mater. Interfaces 2022, 14 (33), 37566–37576. [PubMed: 35939041]

(33). Kumar VB; Kumar R; Gedanken A; Shefi O Fluorescent Metal-Doped Carbon Dots for Neuronal Manipulations. Ultrason Sonochem 2019, 52, 205–213. [PubMed: 30522849]

(34). Singhi SC; Baranwal AK; Jayashree M Acute Iron Poisoning: Clinical Picture, Intensive Care Needs and Outcome. Indian Pediatr 2003, 40 (12), 1177–1182. [PubMed: 14722368]

(35). Baranwal AK; Singhi SC Acute Iron Poisoning: Management Guidelines. Indian Pediatr 2003, 40 (6), 534–540. [PubMed: 12824662]

(36). Mahmoudi M; Simchi A; Milani AS; Stroeve P Cell Toxicity of Superparamagnetic Iron Oxide Nanoparticles. J. Colloid Interface Sci 2009, 336 (2), 510–518. [PubMed: 19476952]

(37). Yu M; Huang S; Yu KJ; Clyne AM Dextran and Polymer Polyethylene Glycol (PEG) Coating Reduce Both 5 and 30 Nm Iron Oxide Nanoparticle Cytotoxicity in 2D and 3D Cell Culture. Int. J. Mol. Sci 2012, 13 (5), 5554–5570. [PubMed: 22754315]

(38). Mahmoudi M; Simchi A; Imani M; Hafeli UO Superparamagnetic Iron Oxide Nanoparticles with Rigid Cross-Linked Polyethylene Glycol Fumarate Coating for Application in Imaging and Drug Delivery. J. Phys. Chem. C 2009, 113 (19), 8124–8131.

(39). Larsen EKU; Nielsen T; Wittenborn T; Birkedal H; Vorup-Jensen T; Jakobsen MH; Ostergaard L; Horsman MR; Besenbacher F; Howard KA; Kjems J Size-Dependent Accumulation of Pegylated Silane-Coated Magnetic Iron Oxide Nanoparticles in Murine Tumors. ACS Nano 2009, 3 (7), 1947–1951. [PubMed: 19572620]

(40). Campos F; Bonhome-Espinosa AB; Carmona R; Durán JDG; Kuzhir P; Alaminos M; López-López MT; Rodriguez IA; Carriel V In Vivo Time-Course Biocompatibility Assessment of Biomagnetic Nanoparticles-Based Biomaterials for Tissue Engineering Applications. Materials Science and Engineering: C 2021, 118, No. 111476. [PubMed: 33255055]

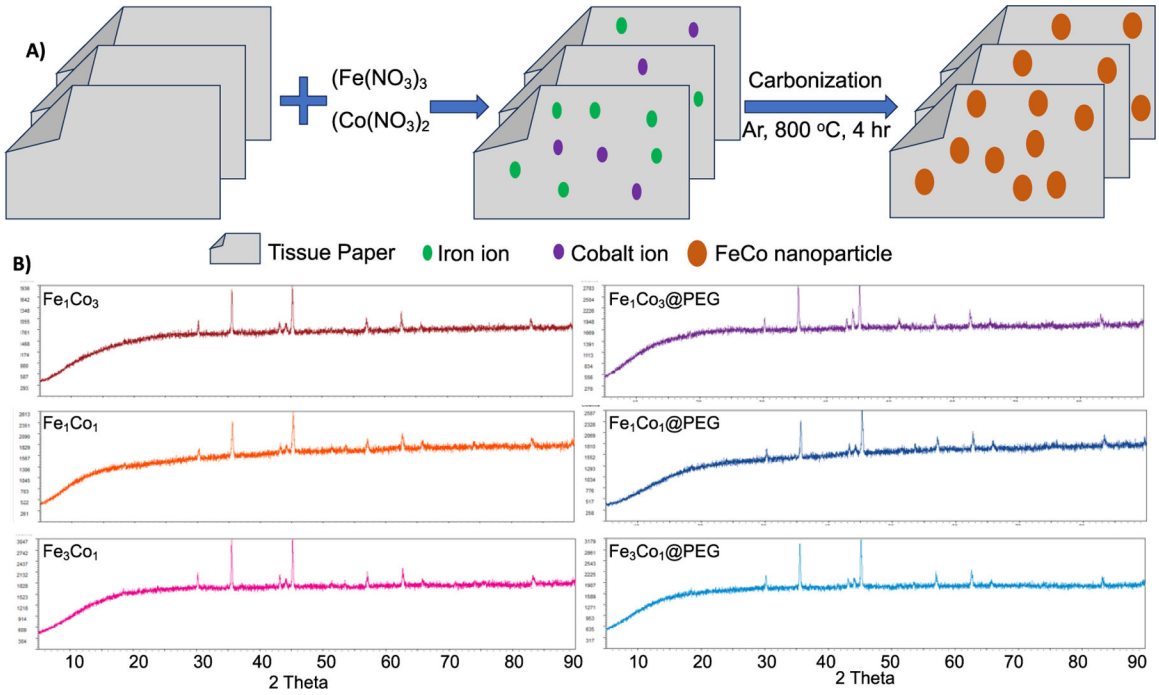

Figure 1.

Preparation and characterization of the particles. (A) The scheme shows the synthetic process and strategy of FeCo/C nanoparticles; (B) XRD pattern of Fe_1Co_3/C Fe_1Co_1/C, and Fe_3Co_1/C nanoparticles, respectively, without (left panel) and with (right panel) PEG coating. No significant changes in their physical properties of the FeCo/C derivatives has been observed after PEG coating.

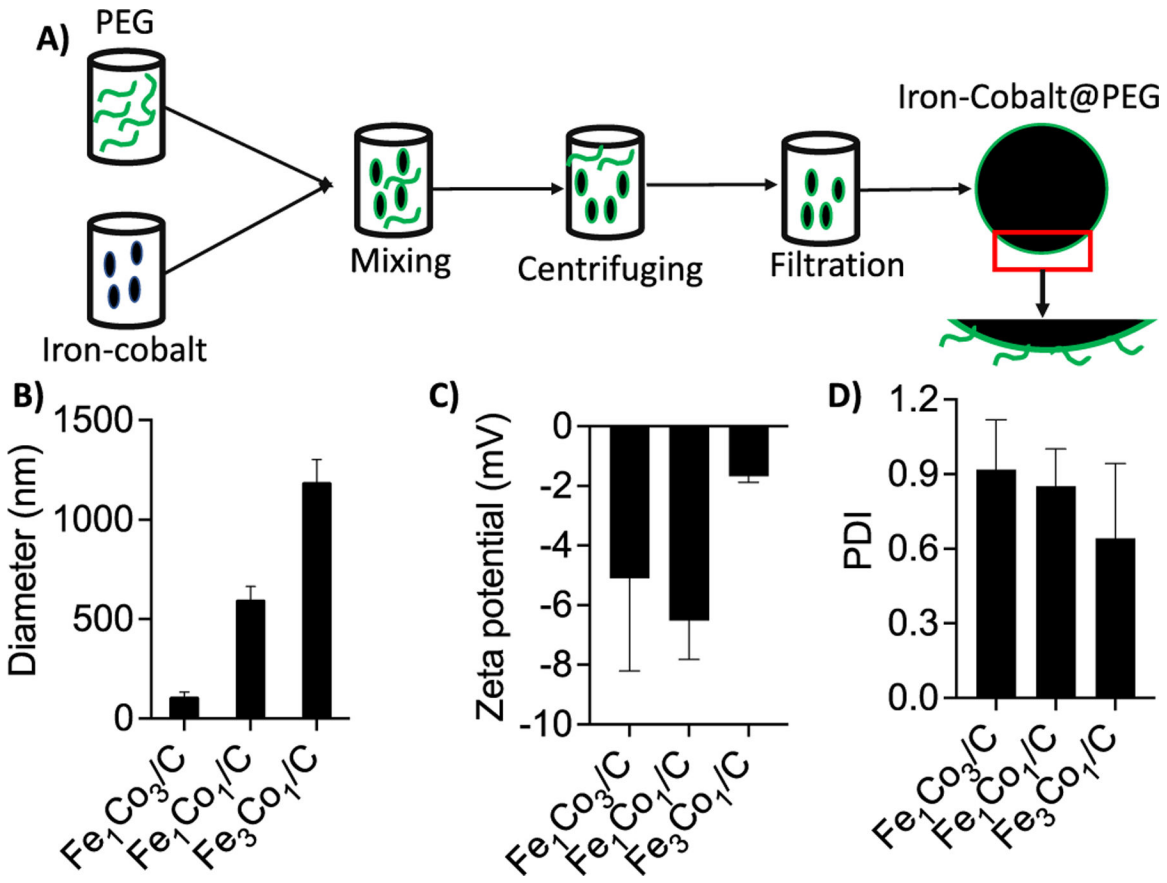

Figure 2.

Surface modification of the particles. Dynamic light scattering analysis of FeCo/C compounds. (A) To enhance aqueous dispersibility, the FeCo/C nanoparticles were coated with PEG. (B) In hydro diameter measurement, we observe an increment of diameter before and after PEG coating for all three compounds. (C) Surface zeta potentials also change due to PEG coating for the FeCo/C compounds. In the FeCo (1:3) compound, zeta potentials change from +6 to −3 mV due to PEG coating. For FeCo (1:1) compound, we also observe more negative zeta from −2 to −6 mV due to PEG coating. (D) In polydispersity index measurement, we found our all three compounds are highly polydisperse and confirmed our compounds are fragmented. Data are presented as mean ± SEM, where $n = 4$.

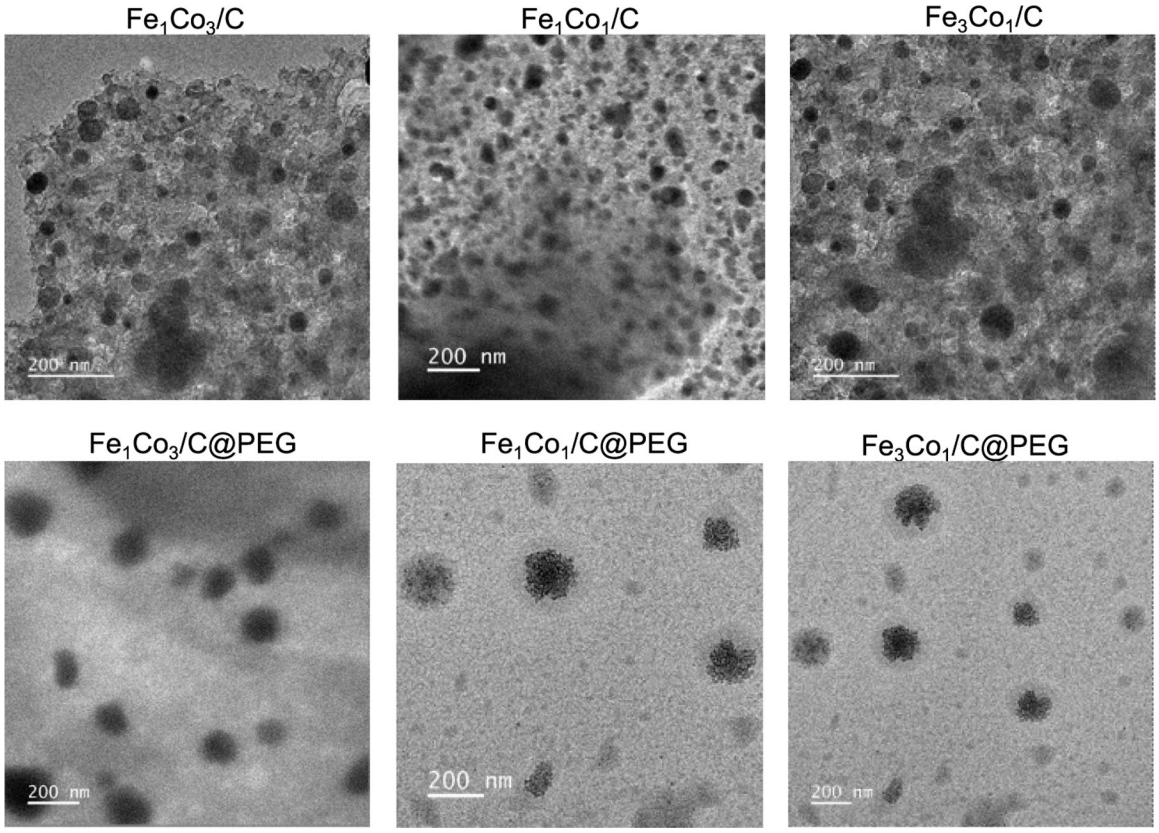

Figure 3.

TEM images of prepared FeCo/C without (upper panel) and with a PEG coating (lower panel). TEM images show PEG coating resulted in a significant increment of particle size as well as dispersibility. Scale bar = 200 nm.

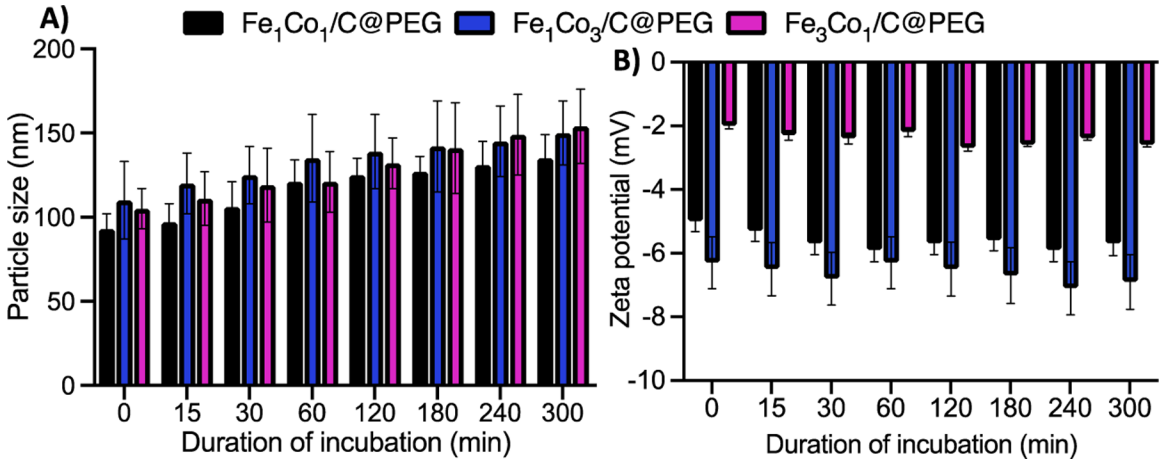

Figure 4.

Stability of PEGylated FeCo/C upon incubation with saline for up to 5 h. Both size distribution (A) and zeta potential (B) of the nanoparticle have been changed on the basis of incubation duration. Data are presented as mean ± SEM, where $n = 3$.

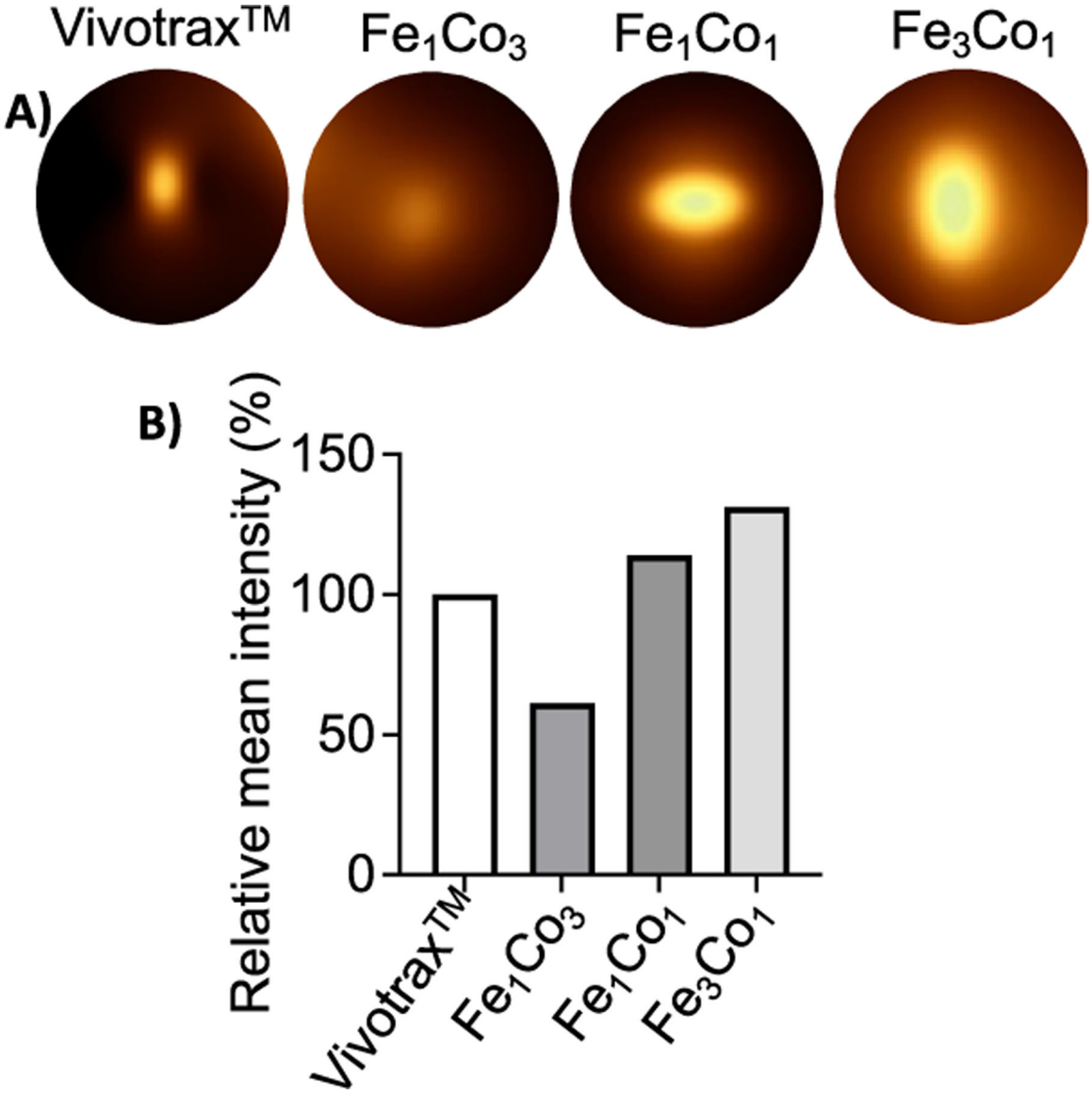

Figure 5.

Magnetic particle imaging. (A) Image of FeCo/C nanoparticles and VivoTrax (Control). (B) Mean intensity of FeCo/C nanoparticle and VivoTrax analyzed by ImageJ. Data is presented as mean ± SEM, where $n = 4$.

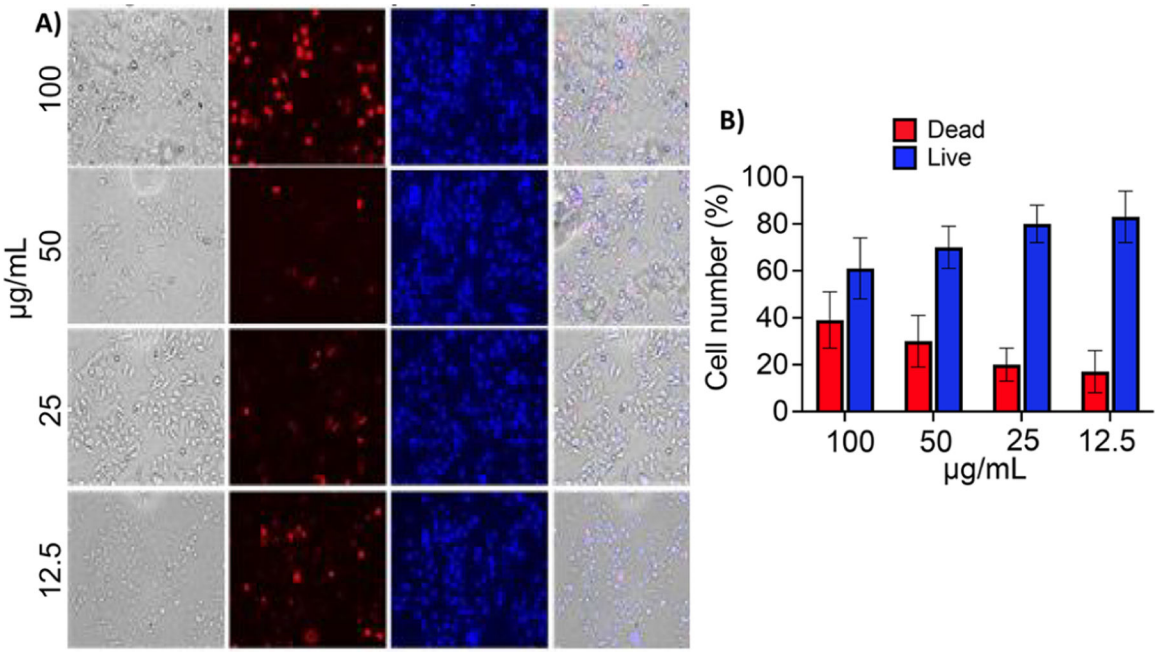

Figure 6.

In vitro biosafety assay. Live–dead assays were performed to evaluate the optimal dose for Fe_1Co_1/C nanoparticles using A375 cells to determine how the Fe_1Co_1/C nanoparticles affect the cells. All images were taken using the EVOS 5000 imaging system and analyzed using ImageJ software to quantify live and dead cells. Scale bars represent 150 μL at 20× magnification. Data is presented as mean ± SEM, where $n = 4$.

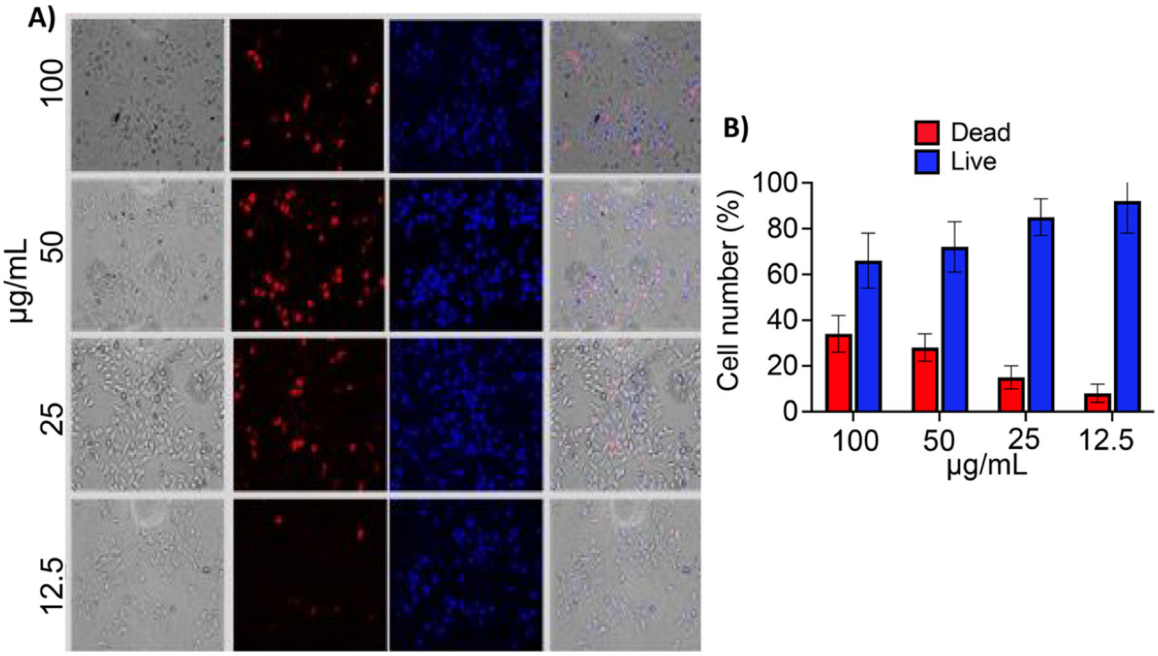

Figure 7.

In vitro biosafety assay. Live–dead assays were performed to evaluate the optimal dose for Fe_1Co_3/C nanoparticles using A375 cells to determine how Fe_1Co_3/C nanoparticles affect the cells. All images were taken using the EVOS 5000 imaging system and analyzed using ImageJ software to quantify live and dead cells. Scale bars represent 150 μL at a 20× magnification. Data is presented as mean ± SEM, where $n = 4$.

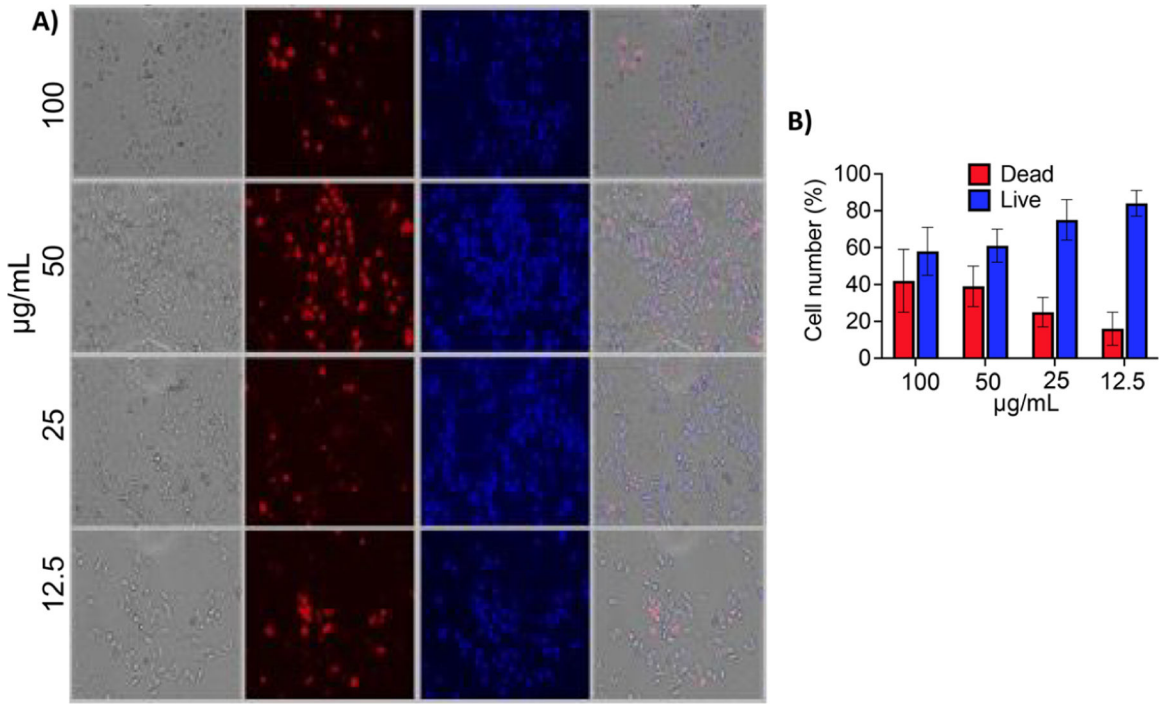

Figure 8.

In vitro biosafety assay. Live–dead assays were performed to evaluate the optimal dose for Fe_3Co_1/C nanoparticles using A375 cells to determine how the Fe_3Co_1/C nanoparticles affect the cells. All images were taken using the EVOS 5000 imaging system and analyzed using the ImageJ software to quantify live and dead cells. Scale bars represent 150 μL at 20× magnification. Data is presented as mean ± SEM, where $n = 3$.

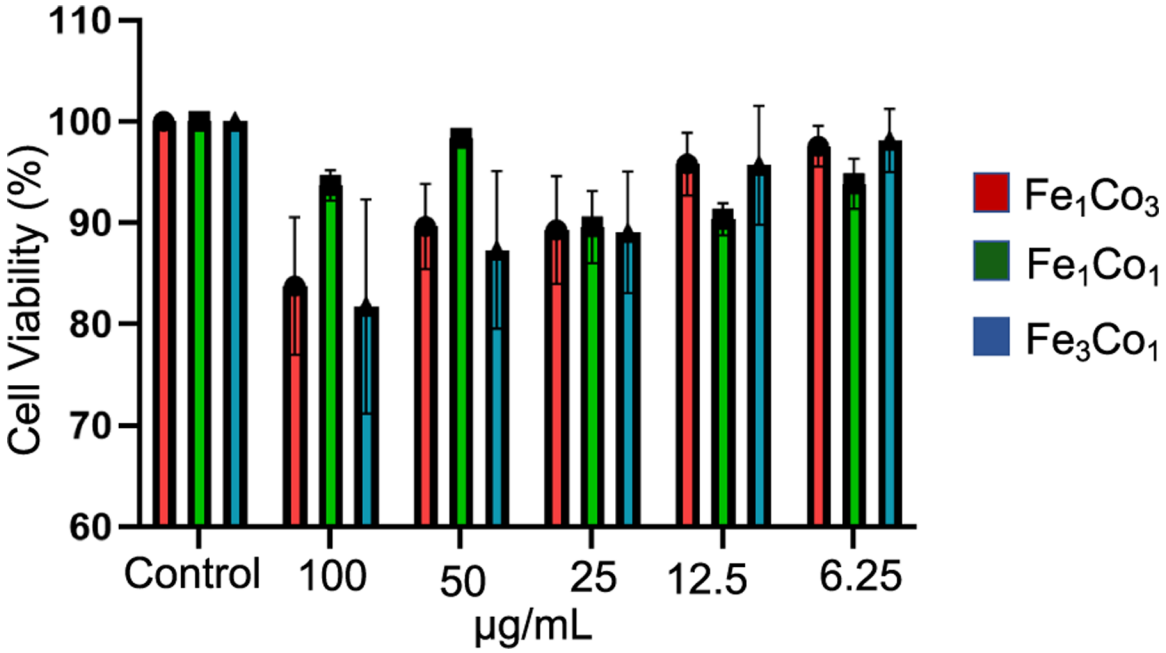

Figure 9.

In vitro cytotoxicity assay. MTT cell viability assay of A375 shows a comparative toxicity profile of various PEGylated iron–cobalt nanoparticles upon coincubation for 6 h. The graph represents cell viability of PEG-coated FeCo/C nanoparticles 6 h treatment at control, 100, 50, 25, 12.5, and 6.25 μg/mL concentration. PEG-coated FeCo/C nanoparticles show lower toxicity compared with uncoated FeCo/C nanoparticles. Data are presented as mean ± SEM, where $n = 6$.

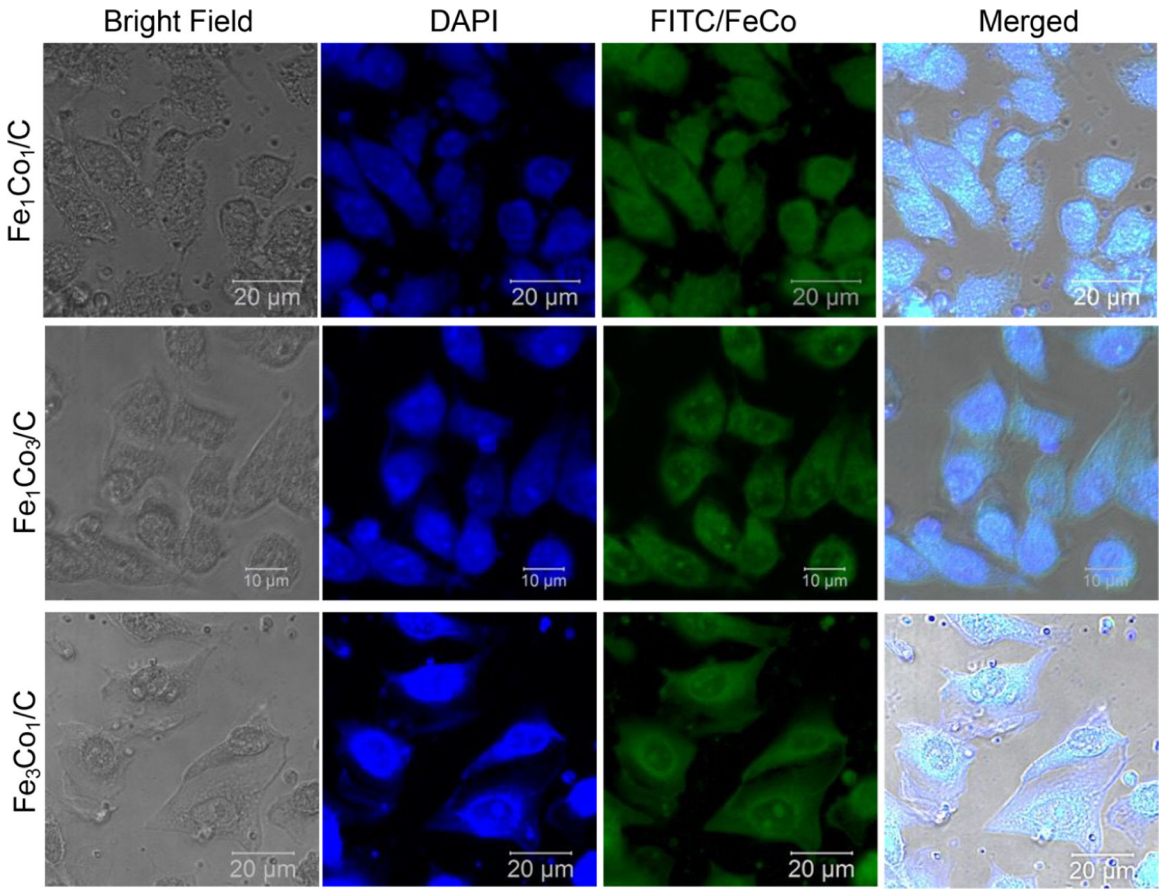

Figure 10.

In vitro cellular uptake profile. RhB fluorescence signal was detected under the microscope in both human lung fibroblasts and A375 cells after 6 h of incubation at 37 °C. All three PEGylated FeCo/C nanoparticles were shown to be up taken by the cell and located inside of the membrane and cell cytoplasm region of A375 cells. Images were taken by EVOS 5000 imaging system at 10× magnification and analyzed by ImageJ software. Scale bars = 20 μm.